# Sensorless Direct Torque Control of Induction Motors Used in Electric Vehicle

Jawad Faiz, Mohammad Bagher Bannae Sharifian, Ali Keyhani, and Amuliu Bogda Proca

***Abstract*—A three-phase squirrel-cage induction motor is used as a propulsion system of an electric vehicle (EV). The motor is controlled at different operating conditions using a direct torque control (DTC) technique combined with a new switching pattern producing low harmonics. The operating flux of the motor is chosen optimally for losses minimization and good dynamic response. Since speed estimation is sensitive to rotor resistance variations, the rotor resistance value is calculated and modified in real time continuously. Simulation and experimental results show that the proposed DTC is able to follow the reference speed (which may be only input reference of the system) with a reasonable dynamic and relatively low error.**

***Index Terms*—DTC control technique, electrical vehicle.**

## I. Introduction

ELECTRIC vehicles are an important step toward solving the environmental problems created by cars with internal combustion engines. Besides energy efficiency and virtually lack of pollution, an advantage of the EV is the availability of electric energy through electric distribution systems. Among disadvantages, EVs have a low energy density and long charging time for the present batteries. Therefore, optimal energy management is very important in EVs; in addition optimum design of the motor, selection of a proper drive, and optimal control strategy are the other major factors in the EVs.

Desired features of the propulsion system (motor) for an EV are high ratio of "torque/inertia" and "power/weight," high maximum torque capability (300–400%), high speed, low level of audible noise, low maintenance, small size, low weight, reasonable cost, high efficiency over low- and high-speed ranges, energy recovery on braking, and nonsensitivity to acceleration forces. Squirrel-cage induction motors have most of the abovementioned features.

Many control techniques have been applied on squirrel-cage induction motors [1]–[6]. Among these techniques, DTC [3], [4], [6], [7] appears to be very convenient for EV applications. The required measurements for this control technique are only the input currents. Flux, torque, and speed are estimated. The input of the motor controller is the reference speed, which is directly applied by the pedal of the vehicle. This paper studies the control of the induction motor used in an EV over different operating regions, above and below the rated speed, using a sensorless DTC technique. A new low-harmonic producing switching pattern is introduced and used in DTC. This switching pattern is based on a nonhysteresis controller having simple logic and, thus, is low cost compared with conventional hysteresis controllers. The flux reference is calculated using the reference speed of the motor at any operating condition. Considering the battery energy limitation, efficiency optimal control is required during steady-state (constant speed) operation. The steady-state optimal control depends on rotor resistance; thus, online identification of this resistance is required [8]. The precise value of stator resistance is needed for DTC. Its value is calculated based on temperature by using a thermal sensor.

The paper is organized as follows. Section II discusses the DTC technique based on the nonhysteresis controllers for flux and torque. Section III is devoted to the computations of synchronous and mechanical speeds. Section IV studies the optimization of the steady-state operation and estimation of the rotor resistance. Sections V and VI show the simulation and experimental results. Section VII is the conclusion.

TABLE I
SWITCHING THE PROPOSED DTC TECHNIQUE

| | N | 1 | 2 | 3 | 4 | 5 | 6 |
|---|---|---|---|---|---|---|---|
| $K_\phi$=1 | $K_T$=1 | 110 | 010 | 011 | 001 | 101 | 100 |
| | $K_T$=0 | 111 | 000 | 111 | 000 | 111 | 000 |
| | $K_T$=-1 | 101 | 100 | 110 | 010 | 011 | 001 |
| $K_\phi$=0 | $K_T$=1 | 010 | 011 | 001 | 101 | 100 | 110 |
| | $K_T$=0 | 000 | 111 | 000 | 111 | 000 | 111 |
| | $K_T$=-1 | 001 | 101 | 100 | 110 | 010 | 011 |

TABLE II
SPECIFICATIONS OF THE PROPOSED INDUCTION MOTOR

| f (Hz) | P (kW) | p | V (V) | $R_s$ (Ω) | $R_r$ (Ω) | $L_s$=$L_r$ (H) | $L_m$ (H) |
|---|---|---|---|---|---|---|---|
| 50 | 1.5 | 2 | 280 | 0.5 | 1.0 | 0.105 | 0.1 |

## II. DTC Technique Using NonHysteresis Controllers for Flux and Torque

The DTC technique is based on the direct stator flux and torque control [3], [4], [6], [7], [9], [10]. The input voltage $(v_s)$ and current $(i_s)$ of the motor on the stationary reference frame can be expressed as

$$v_s = v_{s\alpha} + jv_{s\beta} \tag{1}$$

$$i_s = i_{s\alpha} + ji_{s\beta}. \tag{2}$$

Manuscript received May 4, 2002.

J. Faiz is with the Department of Electrical and Computer Engineering, University of Tehran, Tehran, Iran.

M. B. B. Sharifian is with the Department of Electrical Engineering, University of Tabriz, Tabriz, Iran.

A. Keyhani and A. B. Proca are with the Department of Electrical Engineering, The Ohio State University, Columbus, OH 43210 USA.

Digital Object Identifier 10.1109/TEC.2002.805220

0885-8969/02$17.00 © 2003 IEEE

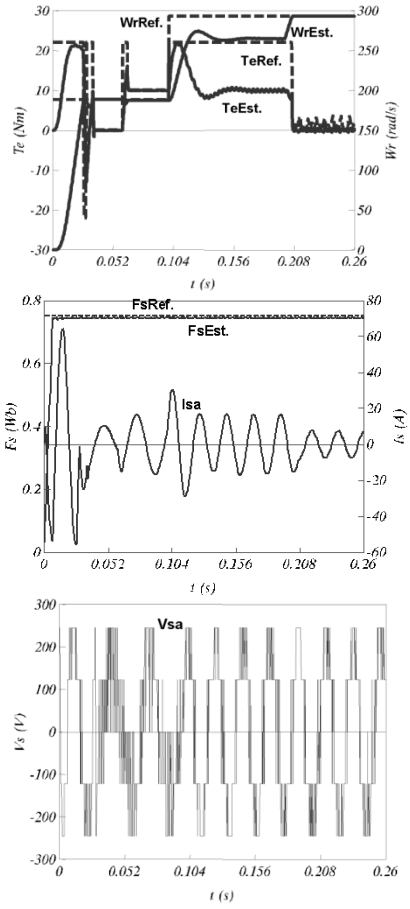


Fig. 1. Torque, speed, flux, current, and voltage variations versus time in the first case.

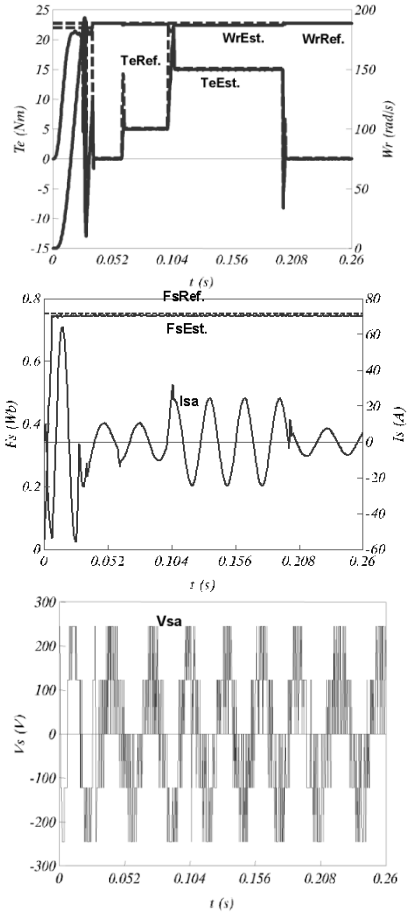


Fig. 2. Torque, speed, flux, current, and voltage variations versus time in the second case.

The actual stator flux can be estimated from the equivalent circuit of the motor as follows:

$$\varphi_s = \int (v_s - R_s i_s)dt + \varphi_{s0} \tag{3}$$

$$\phi_s = \sqrt{\varphi_{s\alpha}^2 + \varphi_{s\beta}^2} \tag{4}$$

where $\varphi_s$ is the flux vector, $\varphi_{s0}$ is the initial flux vector, $\phi_s$ is the flux vector rms value, and $R_s$ is the stator resistance. The electromagnetic torque of the motor is

$$T_e = \varphi_{s\alpha} i_{s\beta} - \varphi_{s\beta} i_{s\alpha}. \tag{5}$$

The control command for the system is speed (by means of the pedal). The flux reference can be calculated based on the speed. Below the rated speed, rated flux is used as a reference (constant torque region). Above the rated speed, a relatively large rated flux may imply the need to exceed the supply voltage limits to maintain speed. Therefore, a flux-weakening method generates the flux reference (constant power region) for higher-than-rated speed. The reference flux is selected, proportional to the inverse of the reference speed [11]. The reference torque can be calculated using the difference between reference speed and instantaneous speed (using a PI controller). However, for a large step in reference speed, the reference torque will be considerably larger than what the motor can develop without exceeding current and/or voltage limits. This result is more obvious over the field-weakening region. In order to reduce this large torque command, a ramp reference speed is employed. Selection of such reference speed improves the dynamic response of the torque and flux control.

Two nonhysteresis controllers are used to control torque and flux [12]. The major advantage of using nonhysteresis controllers is that they are simple compared with PWM types, and they produce fewer harmonics than hysteresis controllers. By proper choice of the control levels (that enable the controller to respond correctly to the errors), it is possible to reduce the parasitic harmonics while maintaining a switching frequency that is considerably lower than that of a PWM technique. The major drawback of the hysteresis controllers (compared with PWM) is that the supply frequency remains unknown. In this technique, the inverter is switched on using the difference between the reference and actual values of the torque and the stator flux; therefore, the stator flux position is over each six control regions of the motor. In PWM, two current or voltage profiles are compared, and based on the error, controlling signals are produced; hence, in the proposed method, no comparison between two similar curves is done. Flux and torque errors are calculated as follows:

$$\Delta\phi = \phi_s^* - \phi_s \tag{6}$$

$$\Delta T = T_e^* - T_e \tag{7}$$

where $\phi_s^*$ and $T_e^*$ are the reference flux and torque, respectively. The switching table is shown in Table I, where $-(\pi/6) + (1 -$

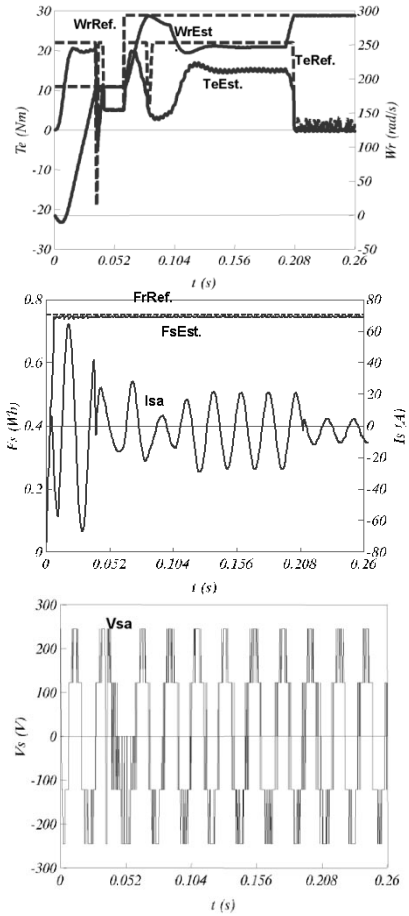


Fig. 3. Torque, speed, flux, current, and voltage variations versus time in the third case.

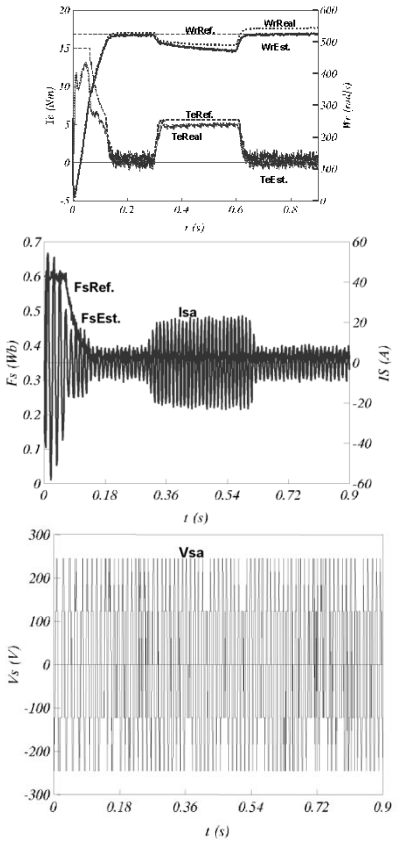


Fig. 4. Torque, speed, flux, current, and voltage variations versus time in the forth case.

$N)(\pi/3) \leq \theta_s(N) < (\pi/6) - (1-N)(\pi/3)$ defines the stator flux position over six regions of motor controlling (60°), and $K_T$ and $K_\phi$ are the torque and flux error coefficients calculated as follows [12]:

$$\begin{aligned} \text{If } \Delta T > \varepsilon_T, \text{ then } K_t &= 1 \\ \text{If } \Delta\phi > \varepsilon_\phi, \text{ then } K_\phi &= 1 \\ \text{If } -\varepsilon_T \leq \Delta T < \varepsilon_T, \text{ then } K_T &= 0 \\ \text{If } \Delta\phi > -\varepsilon_\phi, \text{ then } K_\phi &= 0 \end{aligned}$$

where $\varepsilon_T$ and $\varepsilon\phi$ are the acceptable predefined torque and flux errors, respectively. The stator input voltages are evaluated in order to determine the stator voltage vector. Having the control strategy (switching pattern), the stator voltage vector can be directly calculated as follows:

$$v_s = \sqrt{\frac{2}{3}} V \left( s_a + s_b e^{j(2\pi/3)} + s_c e^{-j(2\pi/3)} \right) \qquad (8)$$

where $V$ is the supply voltage of the inverter (EV battery), and $s_a$, $s_b$, and $s_c$ are numbers 0 or 1 that are the output of the switching table. In fact, they are relevant to the switching strategy and have the following firing commands of the inverter:

$s_i = I(0)$ the phase $i$ is connected to the positive (negative) polarity of the supply

where $i = a, b, c$ defines the phases of the motor supply. In Table I, the three-digit numbers define the switching algorithm where digits from left to right give values of $s_a$, $s_b$, and $s_c$, respectively.

## III. Calculation of Synchronous and Mechanical Speeds

Several methods have been presented to calculate the motor synchronous speed [5], [7], [9], [13], [14]. Most of these methods assume a sinusoidal waveform for the supply voltage. Hence, they are unable to predict synchronous speed for the actual inverter voltage containing high-order harmonics with relatively high amplitudes over different operating conditions. Five methods are summarized in [7]; the authors of this paper use the fourth method. Synchronous speed estimation is based on the rotor flux vector calculation. Both stator and rotor flux vectors rotate with the synchronous speed, but the stator flux is under the influence of the stator voltage and current harmonics. Therefore, in transient modes (where harmonics amplitudes are high), the influence of the harmonics leads to unreal synchronous speed values. However, the harmonic content of the stator voltage and current have less influence on the rotor flux, and its waveform is almost sinusoidal. Since the rotor flux oscillates at synchronous frequency; the synchronous speed can be estimated by calculation of the $\alpha\beta$ components of the rotor flux ($\omega_s = d\theta_r/dt$, where $\theta_r$ is the position of rotor flux). The rotor flux vector can be evaluated using the stator current and flux vectors as follows:

$$\varphi_r = \varphi_{r\alpha} + j\varphi_{r\beta} = \frac{L_m^2 - L_s L_r}{L_m} i_s + \frac{L_r}{L_m} \varphi_s \qquad (9)$$

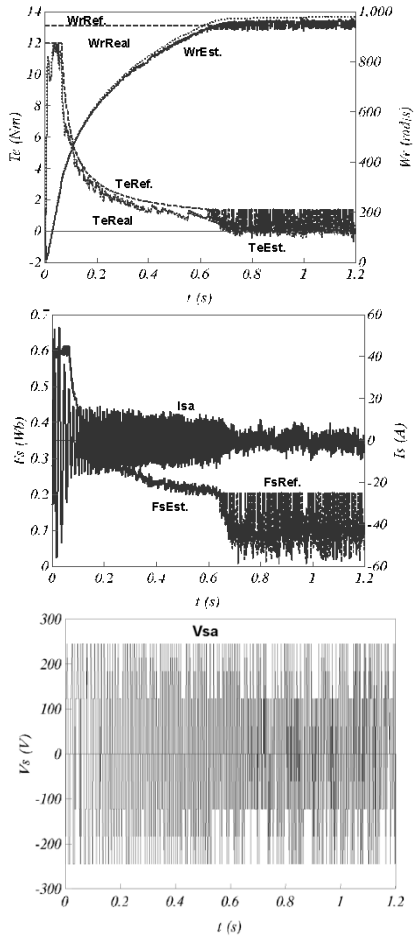


Fig. 5. Torque, speed, flux, current, and voltage variations versus time in the fifth case.

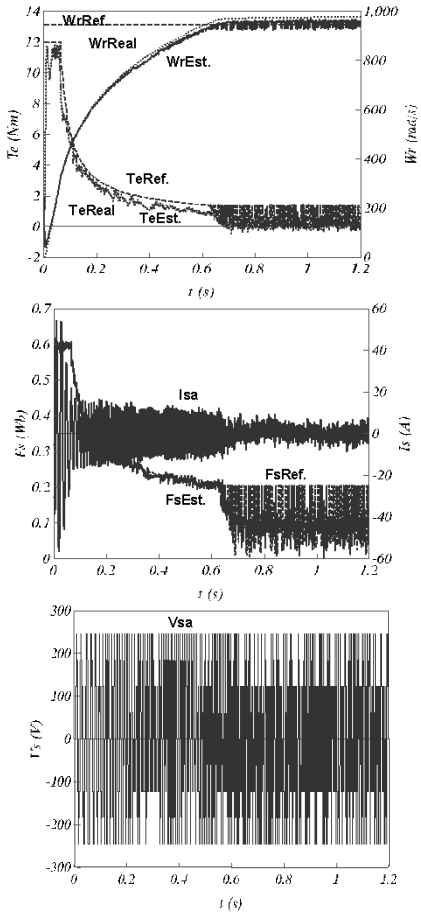


Fig. 6. Torque, speed, flux, current, and voltage variations versus time in the sixth case.

where $L_m$, $L_s$, and $L_r$ are the magnetizing inductance and self-inductance of the stator and rotor, respectively. Many methods have been introduced for rotor-speed estimation [1], [7], [15], [16]. In the present work, the method of [1], [7] is used; slip estimation in transient modes is employed for the evaluation of motor slip and speed.

$$\omega_{\text{slip}} = \frac{R_r T_e}{\phi_r^2} \tag{10}$$

$$\omega_r = \omega_s - \omega_{\text{slip}} \tag{11}$$

where $R_r$ is the resistance of the rotor.

## IV. Steady-State Optimization and Rotor Resistance Estimation

Taking into account the energy limitation of the EV battery, the whole EV system consisting of mechanical energy conversion and relevant controllers must be optimized. Optimization of control during transient operation depends on the control strategy of the torque and flux. The optimum control during steady-state operation (constant speed and torque) consists of the selection of the flux that results in highest efficiency. The ohmic and core losses for steady-state operation of an induction motor are

$$P_{\text{loss}} = R_s I_s^2 + R_r I_r^2 + R_i I_i^2 \tag{12}$$

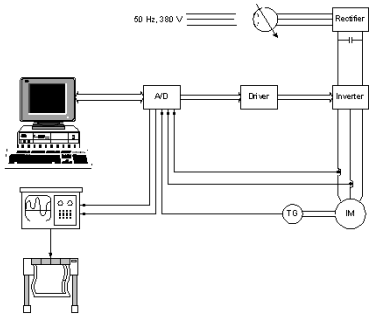


Fig. 7. Experimental set block diagram.

where $I_s$, $I_r$, and $I_i$ are the stator, rotor, and core loss currents, respectively. The equivalent resistance of the core loss is [2]

$$R_i = R_c \left( \frac{\omega_s}{\omega_{s0}} \right)^{1.6} \tag{13}$$

where $R_c$ is the core-loss equivalent resistance at the reference synchronous speed $\omega_{s0}$. Mechanical and inverter losses can be evaluated as

$$P_m = K_m \omega_r^2 \tag{14}$$

$$P_{inv} = K_1 I_s^2 + K_2 I_s \tag{15}$$

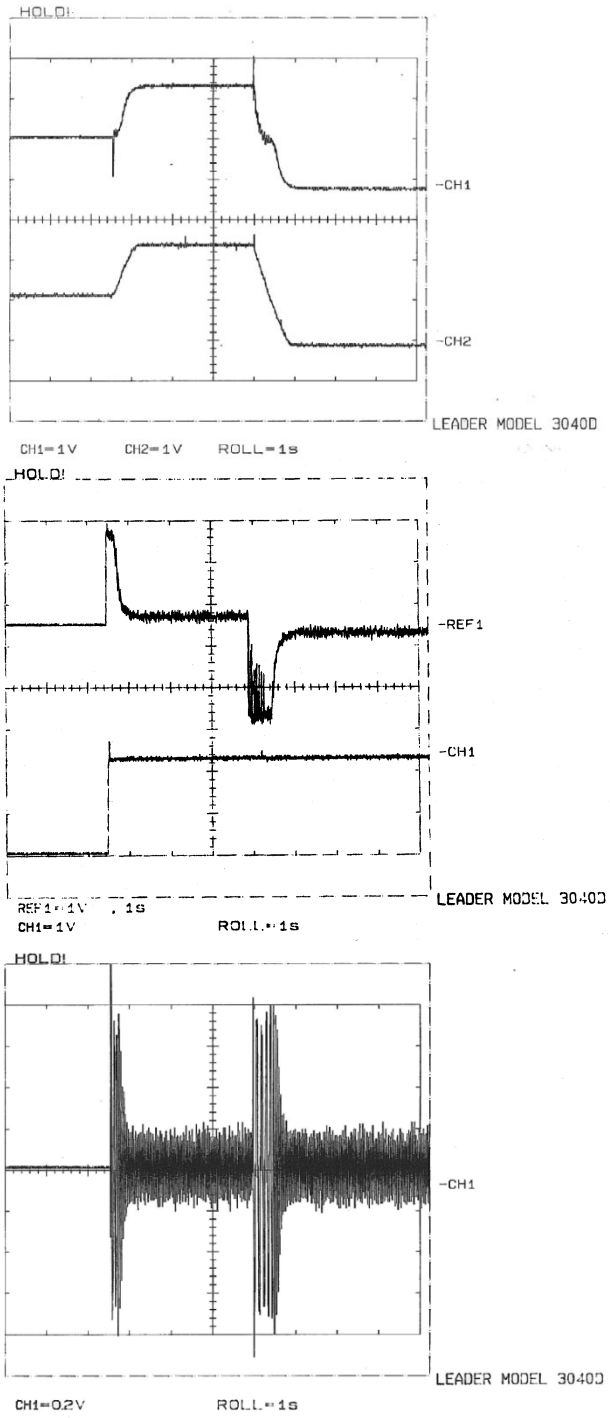


Fig. 8. Experimental results for the conventional algorithm in Case 1. From left to right and up to down: Actual (lower), estimated (upper) speeds. Torque (upper), flux (lower). Current.

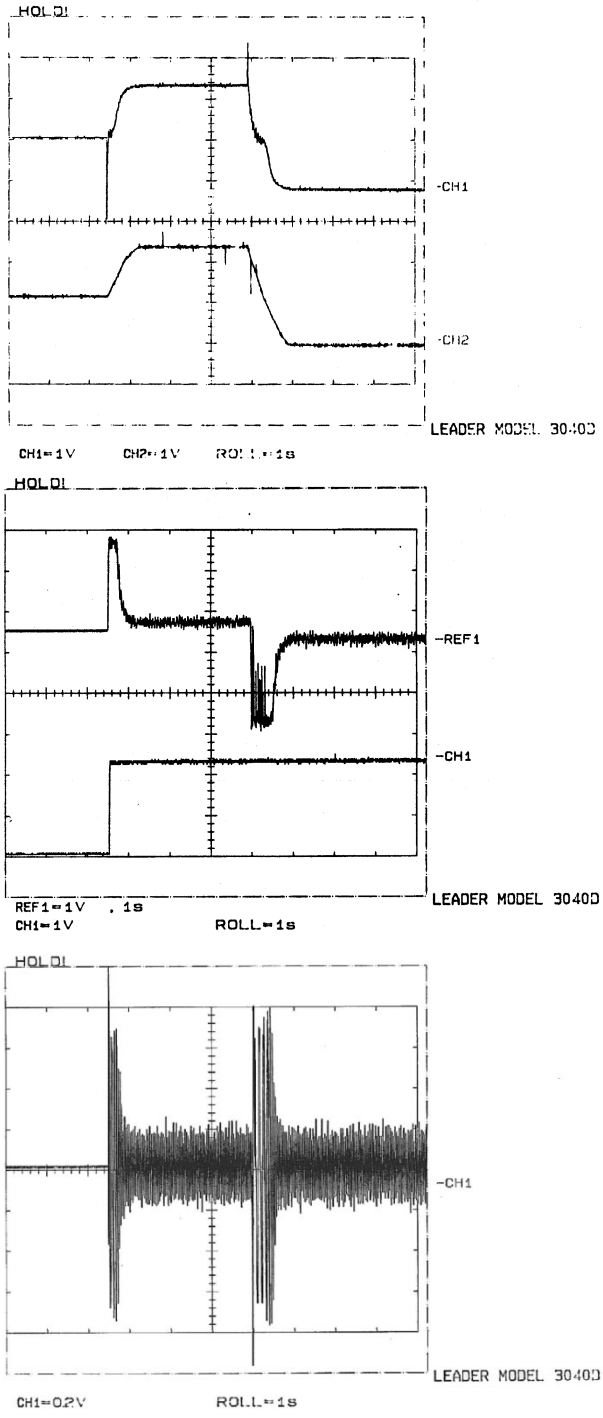


Fig. 9. Experimental results for the proposed algorithm in Case 1. From left to right and up to down: Actual (lower), estimated (upper) speeds. Torque (upper), flux (lower). Current.

where $K_m$, $K_1$, and $K_2$ are constants of the mechanical and inverter losses, respectively. $K_m$ is calculated by the mechanical losses of the motor, and $K_1$ and $K_2$ are evaluated from the electrical specifications of the switching elements. Since the mechanical losses are constant for constant speed, they have no influence on the steady-state optimum flux selection. In the optimum flux calculation, the inverter losses can also be ignored. By transforming the current variables into the stator flux variables (on the base of the flux-current equation of the induction motor) and equating the derivation of the losses versus flux to zero, the following equation is obtained for the stator: Optimum flux during steady-state operation:

$$\phi_s = \sqrt{T_e}\frac{\frac{L_s}{L_m}\sqrt{(A+2B)\frac{L_sL_r-L_m^2}{L_s}}}{(AB+B^2)^{0.25}} \tag{16}$$

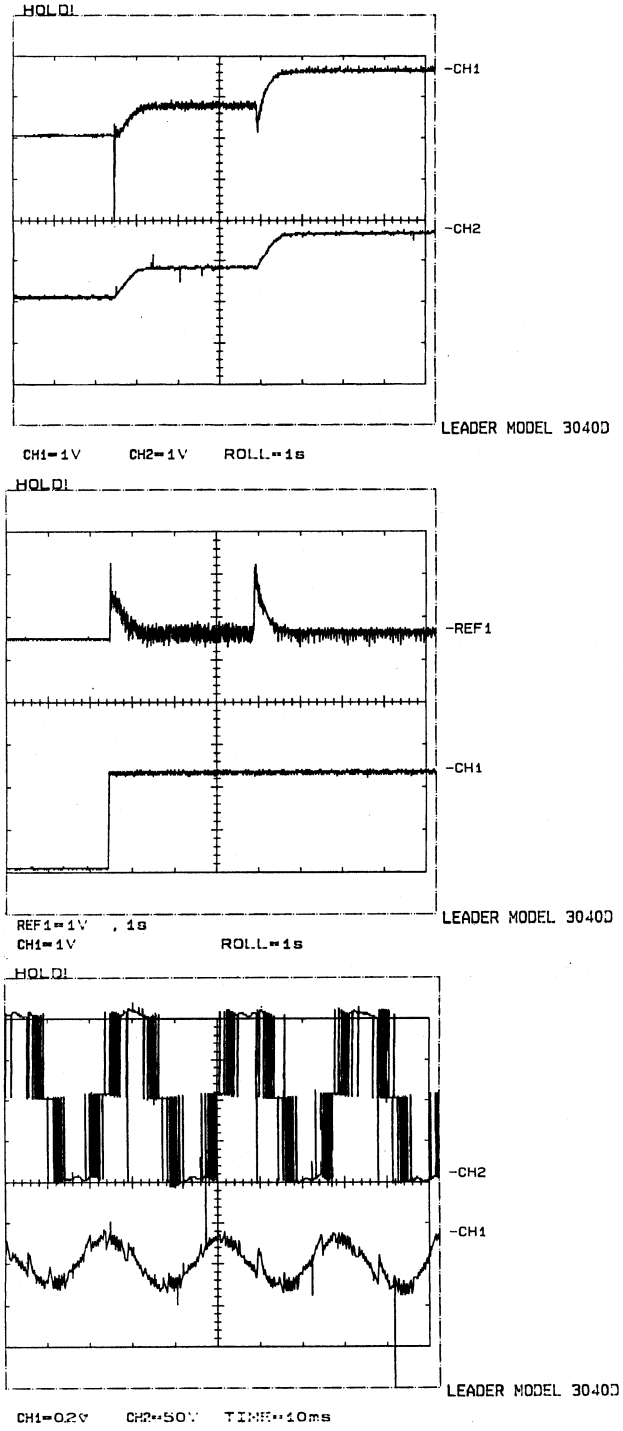


Fig. 10. Experimental results for the conventional algorithm in Case 2. From left to right and up to down: Actual (lower), estimated (upper) speeds. Torque (upper), flux (lower). Current.

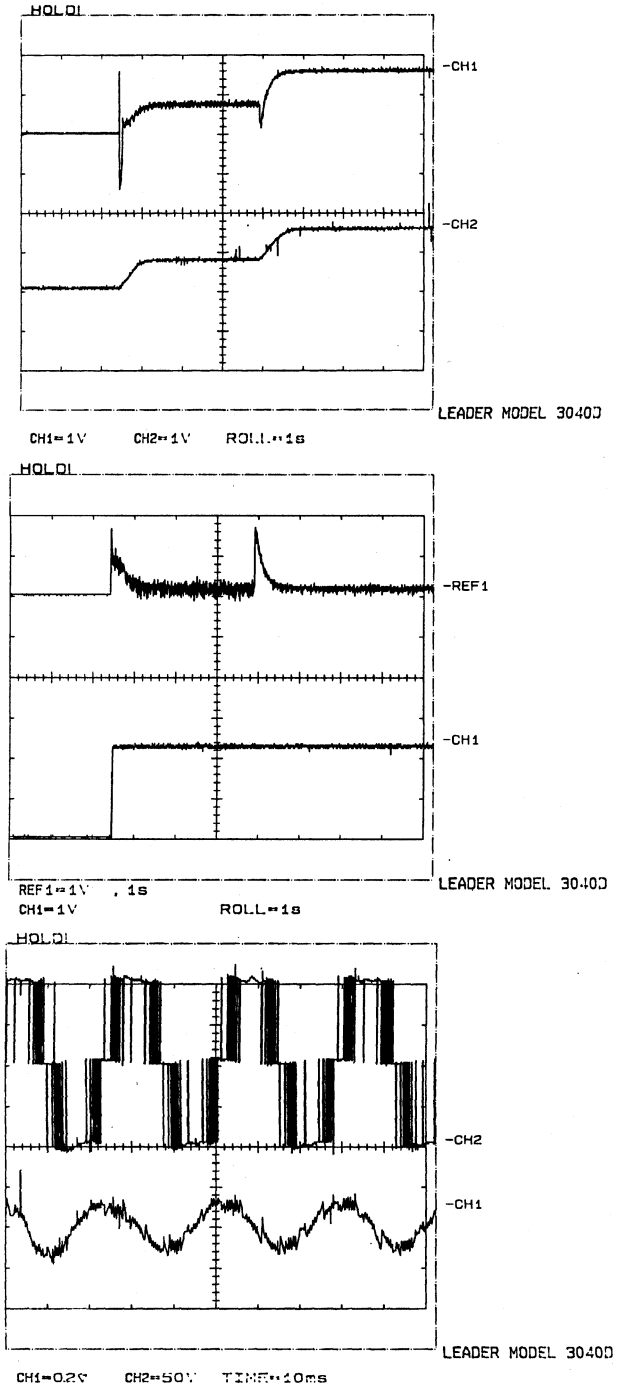


Fig. 11. Experimental results for the proposed algorithm in Case 2. From left to right and up to down: Actual (lower), estimated (upper) speeds. Torque (upper), flux (lower). Current.

where

$$A = \frac{L_m}{L_s L_r - L_m^2}\left[L_s(R_s + R_r)\frac{L_s(L_s L_r - L_m^2)}{L_m^2} + 2R_s\right]$$
$$B = R_s + R_i.$$

The optimum stator flux depends on the six parameters of the equivalent circuit of the motor. The motor operates below the rated speed at the rated flux and above the rated speed with the optimal flux (weakened). Since the optimal flux is usually lower than the rated for this application, there is no magnetic saturation, and parameters $L_s$, $L_r$, and $L_m$ are approximately constant. Only two parameters $R_s$ and $R_r$ must be estimated and modified online [13], [14], [17], [18]. Since sensorless control is sought, synchronous speed, mechanical speed, and motor torque must be estimated. Since the measured quantities are two-phase currents, both resistances $R_s$ and $R_r$ cannot be estimated. A thermal sensor needs to be used in the stator winding in order

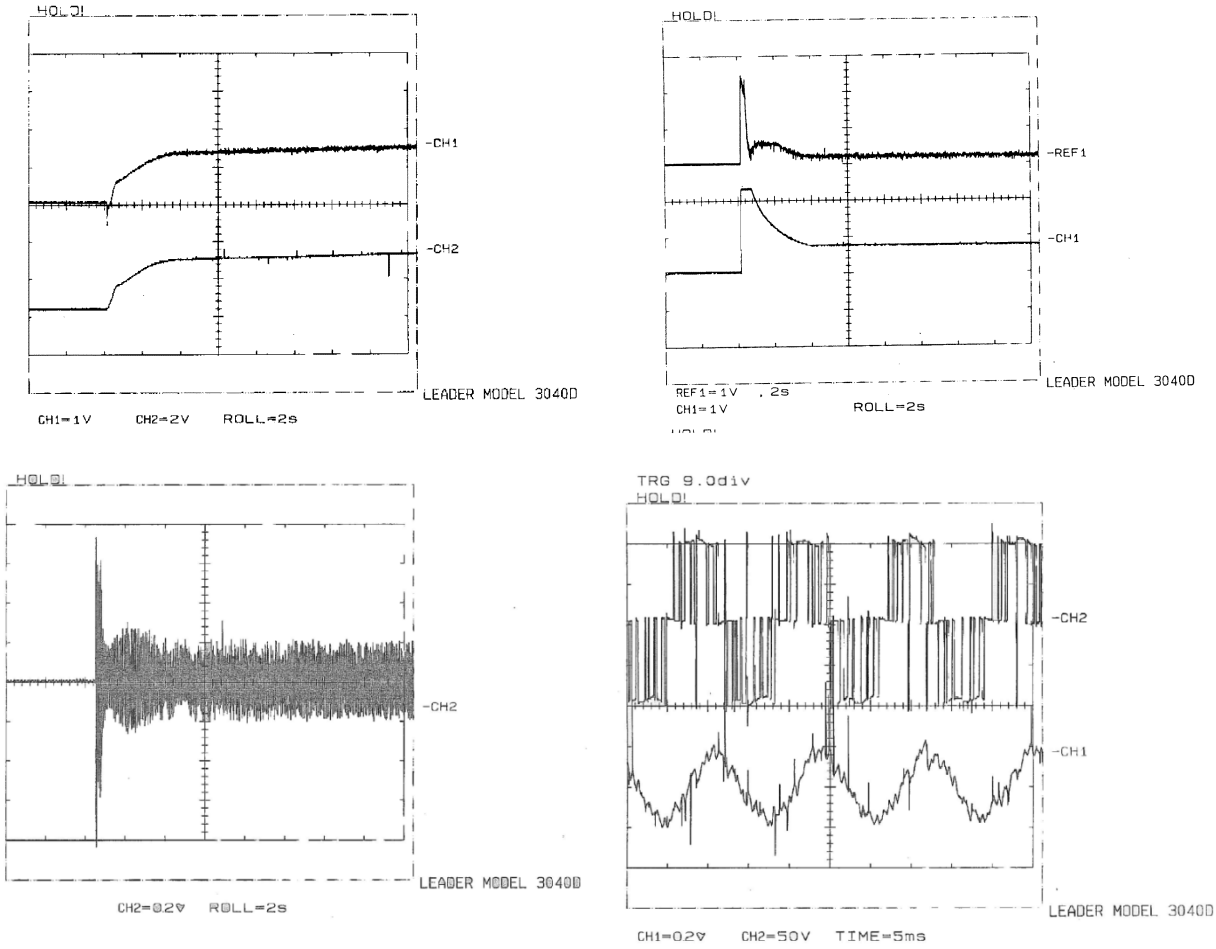


Fig. 12. Experimental results for the conventional algorithm in case 3. From left to right and up to down: actual (lower), estimated (upper) speeds; torque (upper), flux (lower); current; steady-state voltage (upper), current (lower).

to calculate and update the $R_s$ value. Hence, only the estimation of $R_r$ is required. $R_r$ can be estimated based on sensitivity of torque, reactive power, or other motor characteristics versus parameter $R_r$ [8].

## V. Simulation Results—DTC Technique Evaluation

Table II summarizes the specifications of a proposed three-phase induction motor.

Six different operating conditions for simulation are used in order to evaluate motor performance under the proposed control technique.

Case 1) Fig. 1 presents the corresponding curves for the free acceleration of the motor with reference speed equal to 1800 r/min. A load of 10 Nm is applied to the motor at $t = 0.06$ s. A new reference speed equal to 2800 r/min is applied at $t = 0.1$ s. The motor load is dropped at $t = 0.2$ s. Where WrRef, TeRef, FsRef, WrEst, TeEst, and FsEst are the reference and estimated speed, torque, and stator flux, Isa and Vsa are $\alpha$ axis stator current and voltage. The speed reference cannot be followed with load on. The limitation of the developed torque of the motor at 2800 r/min is visible on the torque curve.

Case 2) The characteristics of the motor for free acceleration of the motor with a reference speed of 1800 r/min, applying the load of 5 Nm at $t = 0.06$ s, increasing the load to 15 Nm at $t = 0.1$ s, and finally removing the load at $t = 0.2$ s are shown in Fig. 2. Applying a load equal to 5 Nm at $t = 0.06$ s leads to a quick reaction of the controller, and despite the effect on torque, voltage, and current curves, there is no influence on the speed curve. The increase of load to 15 Nm causes instantaneous reduction of speed; however, the speed controller again approaches the reference speed and follows it.

Case 3) A reference speed of 1800 r/min is applied to the motor loaded with 5 Nm (see Fig. 3). The reference speed is increased to 2800 r/min at $t = 0.06$ s, the load torque is increased to 15 Nm at $t = 0.1$ s, and finally, the motor is unloaded at $t = 0.2$ s. Increasing the load to 15 Nm at $t = 0.1$ s reduces the speed below the reference level due to the limitation of the motor's developed torque.

In cases 1–3, the measured speed was used in the speed controller (not estimated speed), whereas rotor resistance $R_r$ was assumed constant (no estimation). The flux weakening method is used if speed rises

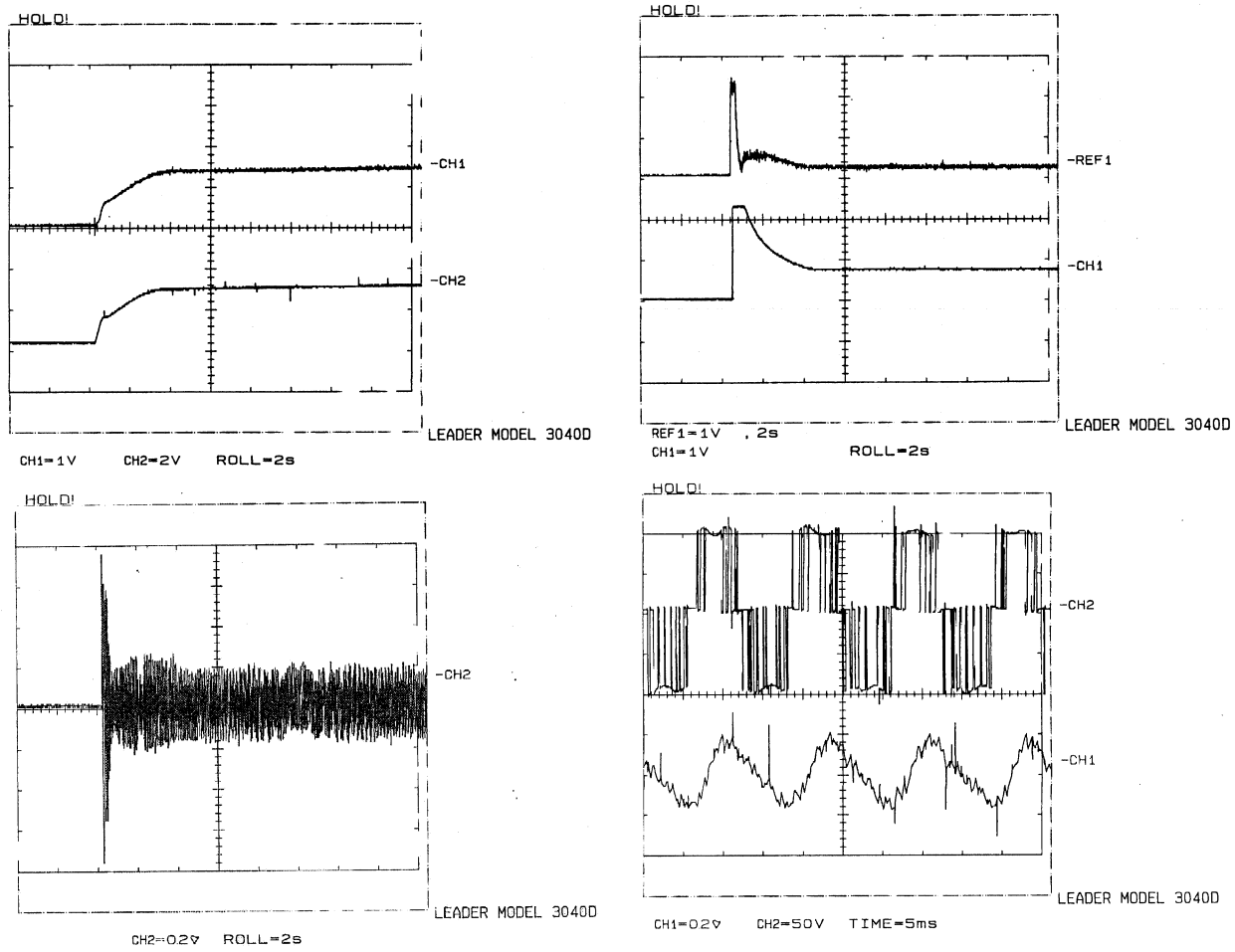


Fig. 13. Experimental results for the proposed algorithm in case 3. From left to right and up to down: actual (lower), estimated (upper) speeds; torque (upper), flux (lower); current; steady-state voltage (upper), current (lower).

above the rated value. In the following cases, the motor is analyzed above the rated speed, and the estimated speed is used in the speed controller (not measured speed).

Case 4) The no-load motor begins with reference speed equal to 5000 r/min. A load of 5 Nm is applied at $t = 0.3$ s and removed at $t = 0.6$ s. In Fig. 4, WrReal and TeReal are the real speed and torque, respectively. For a rapid dynamic operation above the rated speed, the reference flux is not calculated based on the step reference speed; flux is reduced (ramp) with a gradual increase of speed. Application of such reference flux will clearly show its effect on the current and voltage curves (frequency of voltage and current increase of approximately linearly ramp). The speed approaches 5000 r/min from zero over a period shorter than 150 ms. The speed is smooth without fluctuations during the starting period. Large changes of the flux during the initial period of starting lead to a nonaccurate estimation of the synchronous speed, which produces errors in the mechanical speed estimation. However, this error is eliminated in the first few milliseconds.

Case 5) The results of flux optimization during the steady-state operation with 9000-r/min reference speed and a free acceleration are shown in Fig. 5. Flux optimization during the steady-state operation can considerably reduce the flux amplitude and input currents of the motor. This improves the efficiency of the motor. Speed fluctuations at high speed and steady state are present on the curves. Since the amplitude of the reference flux is low, the developed torque of the motor is rapidly reduced, which leads to the fluctuations mentioned before. The optimum flux is automatically chosen. If the speed error is lower than the predefined value, the system optimizes the reference flux automatically; if the error is outside this limit, the reference flux is determined based on the optimal dynamic of the motor. This is the other reason for the increase of flux and speed fluctuations.

Case 6) Fig. 6 shows the free-acceleration of the motor with reference speed equal to 9000 r/min and a rotor resistance with $-10\%$ error. The rotor resistance is estimated in real time, and rotor resistance approaches from 0.9 $\Omega$ (with error) to the actual value of 1 $\Omega$

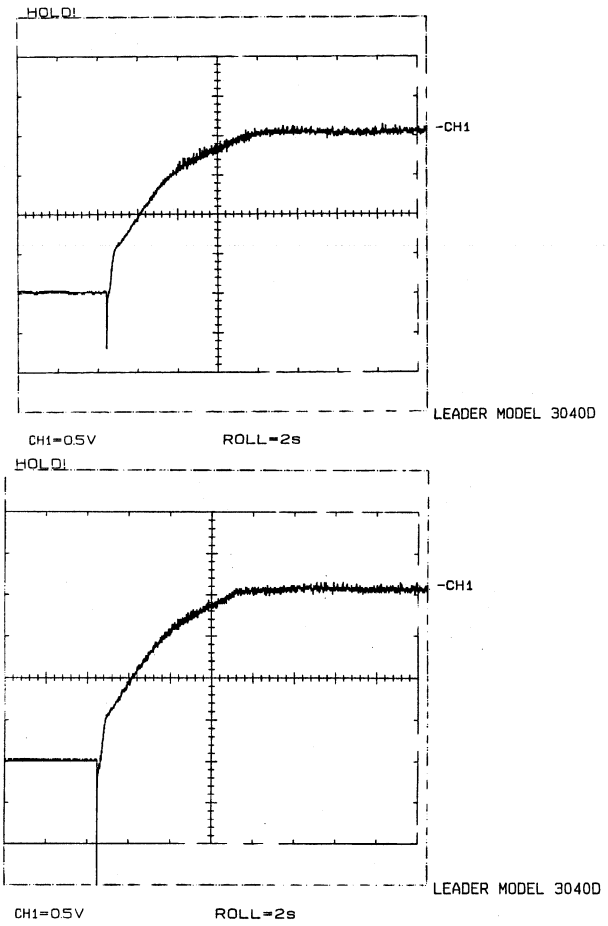


Fig. 14. Estimated speeds for conventional (left) and proposed (right) algorithms in case 4.

in 200 ms. Rotor resistance error shows its small influence on the torque during the initial instants of the starting. This error has almost no effect on the flux of the motor due to the direct calculation of the stator flux using the measured input currents. However, the rotor resistance error induces a speed error during the initial instants of the starting period.

## VI. Experimental Validation

An experimental setup was arranged in order to test the validity of the simulation results.

Fig. 7 shows the experimental set of the motor controlled by DTC. The input dc voltage of the inverter is supplied by a set of rectifiers and autotransformers. Samples of two phases currents are fed to the computer via an analog-to-digital converter. The sampled speed is measured for comparison of the estimated and actual speeds and has no effect in the control routine.

A 5.5-hp, 50-Hz, four-pole induction motor is controlled in some operating conditions using the proposed switching pattern and conventional switching pattern of [19]. The switching frequency for both algorithms is 11 kHz.

Case 1) Figs. 8 and 9 show the experimental curves that result from the conventional and proposed algorithms, respectively, when the motor is starting with reference speed of 800 r/min, and then, the reference speed becomes $-800$ r/min at $t = 3.5$ s.

Case 2) Figs. 10 and 11 show the experimental curves using the conventional and proposed algorithms, respectively, when the motor is started with a reference speed of 600 r/min increased to 1200 r/min at $t = 3.4$ s.

Case 3) If the motor is started using reference speed 2500 r/min, the experimental results of the two control algorithms are shown in Figs. 12 and 13.

Case 4) If the motor is started using reference speed 2800 r/min, the estimated speeds of the motor based on the two control algorithms are as in Fig. 14.

The results show that the proposed algorithm has an advantage over the conventional algorithm with smaller torque, flux, and current ripples. In addition, amplitude of currents using the proposed algorithm is smaller than that of the conventional algorithm (case 3); therefore, its efficiency is better, and the motor's audible noises are lower. On the other hand, this algorithm has smaller harmonics in the input currents, as well as in the flux and developed torque.

## VII. Conclusions

The DTC technique has been employed for the speed control of an induction motor, above and below the rated speed. The input of the control system is the speed reference provided by the pedal of the EV. The required measurements are currents of two phases of the motor. The value of the battery voltage and instantaneous values of the control signals of the inverter $s_a$, $s_b$, and $s_c$ can be used in the place of the measured voltages. Nonhysteresis controllers were used to control torque and flux independently.

The unknown synchronous speed (frequency of the voltage and current) of the motor has been also estimated. During the initial instants of starting, the estimation of the synchronous speed has errors due to the instability of the fluxes; this error leads to errors in the estimated speed. However, this error diminished rapidly. Application of the nonhysteresis controllers leads to the independent control of flux and torque over the known and predefined transient regions. Application of a ramp for flux weakening over the high-speed ranges optimizes the dynamic response of the motor above the rated speed, and the motor approaches the new reference over short intervals. High torque and estimated synchronous speed fluctuations above rated speeds cause fluctuations of the estimated speed of the motor. To reduce these fluctuations, lowpass filters were used in the outputs of the speed (synchronous and mechanical) calculators.

Use of the optimum flux during the steady-state operation of the motor can reduce the amplitude of the current and flux and improve the efficiency. However, this causes fluctuations of the estimated torque and the developed torque. It should be noted that another reason for fluctuations is automatic choice of reference flux between optimum and rated flux. The flux changes between the optimum efficiency and optimal dynamic flux values and produces large fluctuations during steady-state operation.

This can be reduced by nonautomatic choice of the optimum flux.

The control technique is capable of operating over four quadrants (increase and decrease of speed in positive and negative directions). During braking, the kinetic energy of the EV is partially recovered and returned to the batteries, which improves the total efficiency of the system.

The proposed algorithm has smaller harmonics and current amplitude than the conventional method, which improves the total system efficiency and other parasitic noises.

## REFERENCES


[1] U. D. Choiet *et al.*, "A high efficiency drive system for electric vehicle," *IEVS-13*, pp. 537–543, 1996.

[2] K. Matsus and S. Katsuta, "Fast rotor flux control of vector controlled induction motor operating at maximum efficiency for electric vehicles," *IEVS-13*, pp. 272–278, 1996.

[3] J. Faiz *et al.*, "Direct torque control of induction motor for electric propulsion systems," *Int. J. Elect. Power Syst. Res.*, vol. 51, pp. 95–101, Aug. 1999.

[4] U. Baader, M. Depenbrock, and G. Gierse, "Direct self control (DSC) of inverter-fed induction machine: A basis for speed control without speed measurement," *IEEE Trans. Ind. Applicat.*, vol. 28, pp. 581–588, May/June 1992.

[5] O. Kukrer, "Discrete-time current control of voltage-fed three-phase PWM inverter," *IEEE Trans. Power Electron.*, vol. 11, pp. 260–269, Mar. 1996.

[6] T. G. Habetler *et al.*, "Direct torque control of induction machines using space vector modulation," *IEEE Trans. Ind. Applicat.*, vol. 28, pp. 1045–1053, Sept./Oct. 1992.

[7] P. Vas, *Sensorless Vector and Direct Torque Control*. New York: Oxford Univ. Press, 1998.

[8] J. Faiz and M. B. B. Sharifian, "Different techniques for real time estimation of an induction motor rotor resistance sensorless DTC for EV," *IEEE Trans. Energy Conversion*, vol. 16, pp. 104–109, Mar. 2001.

[9] I. Takahashi and Y. Ohmori, "High-performance direct torque control of an induction motor," *IEEE Trans. Ind. Applicat.*, vol. 25, pp. 257–264, Mar./Apr. 1989.

[10] T. G. Habetler and D. M. Divan, "Control strategies for direct torque control using discrete pulse modulation," *IEEE Trans. Ind. Applicat.*, vol. 27, pp. 893–901, Sept./Oct. 1991.

[11] X. Xu and D. W. Novotny, "Selection of the flux reference for induction machine drives in the field weakening region," *IEEE Trans. Ind. Applicat.*, vol. 28, pp. 1353–1358, Nov./Dec. 1992.

[12] J. Faiz, M. B. B. Sharifian, and V. Fedak, "Minimization of current harmonics of DTC controller using a suitable switching pattern," in *Proc. Ninth Int. Conf. Power Electron. Motion Cont.*, vol. 3, Kosice, Slovak Republic, 2000, EPE-PEMC 2000, pp. 161–166.

[13] T. Matsuo and T. A. Lipo, "A rotor parameter identification scheme for vector-controlled induction motor drives," *IEEE Trans. Ind. Applicat.*, vol. IA-21, pp. 624–632, July/Aug. 1985.

[14] H. Sugimoto and S. Tamai, "Secondary resistance identification of an induction-motor applied model reference adaptive system and its characteristics," *IEEE Trans. Ind. Applicat.*, vol. IA-23, pp. 296–303, Mar./Apr. 1987.

[15] N. P. Rubin, R. G. Harley, and G. Diana, "Evaluation of various slip estimation techniques for an induction machine operating under field-oriented control conditions," *IEEE Trans. Ind. Applicat.*, vol. 28, pp. 1367–1375, Nov./Dec. 1992.

[16] C. M. Lee and C. L. Chen, "Observer-bared speed estimation method for sensorless vector control of induction motor," in *Proc. IEEE Contro. Theory Applicat.*, vol. 145, 1998, pp. 359–363.

[17] M. Koyama *et al.*, "Microprocessor-based vector control system for induction motor drives with rotor time constant identification function," *IEEE Trans. Ind. Applicat.*, vol. IA–22, pp. 453–459, May/June 1986.

[18] L. Umanand and S. R. Bhat, "On-line estimation of stator resistance of an induction motor for speed control applications," *Proc. Inst. Elect. Eng.. Electr. Power App.*, vol. 142, no. 2, pp. 97–103, 1995.

[19] I. Takahashi and T. Noguchi, "An new quick-response and high-efficiency control strategy of an induction motor," *IEEE Trans. Ind. Applicat.*, vol. IA-22, pp. 820–827, Sept./Oct. 1986.



**Jawad Faiz** received the Ph.D. degree in electrical engineering from the University of Newcastle-upon-Tyne, Newcastle-upon-Tyne, U.K., in 1988.

Currently, he is Professor of electrical engineering with the Department of Electrical and Computer Engineering, University of Tehran, Tehran, Iran. He was also an Assistant Professor with the Department of Electrical Engineering, University of Tabriz, Tabriz, Iran, where he has been since 1988. His reserch interests include induction motor design, modeling, and applications.

**Mohammad Bagher Bannae Sharifian** received the Ph.D. degree in electrical engineering from Tabriz University, Tabriz, Iran, in 2000.

Currently, he is Assistant Professor of electrical engineering at Tabriz University. His research interests include induction motor design, modeling, control and applications, transformers, switched reluctance motor modeling, and reactive-power control.

**Ali Keyhani** received the Ph.D. degree from Purdue University, West Lafayette, IN, in 1975.

Currently, he is Professor of electrical engineering at The Ohio State University, Columbus. His research interests include control and modeling, parameter estimation, failure detection of electric machines, transformers, and drive systems.

**Amuliu Bogdan Proca** received the degree in electrical engineering from Politechnica University of Bucharest, Bucharest, Romania, in 1992 and the M.S.E.E. and Ph.D. degrees from The Ohio State University, Columbus, in 2000.

His research interests include the areas of induction machine control, modeling, parameter estimation, and design.